Journal of Cerebral Blood Flow & Metabolism (2013) 33, 612–618

www.jcbfm.com

ORIGINAL ARTICLE

# Multivariate spatial covariance analysis of $^{99m}$Tc-exametazime SPECT images in dementia with Lewy bodies and Alzheimer's disease: utility in differential diagnosis

Sean J Colloby[1], John-Paul Taylor[1], Christopher M Davison[1], Jim J Lloyd[2], Michael J Firbank[1], Ian G McKeith[1] and John T O'Brien[3]

We examined $^{99m}$Tc-exametazime brain blood flow single-photon emission computed tomography (SPECT) images using a spatial covariance analysis (SCA) approach to assess its diagnostic value in distinguishing dementia with Lewy bodies (DLB) from Alzheimer's disease (AD). Voxel SCA was simultaneously applied to a set of preprocessed images (AD, $n = 40$; DLB, $n = 26$), generating a series of eigenimages representing common intercorrelated voxels in AD and DLB. Linear regression derived a spatial covariance pattern (SCP) that discriminated DLB from AD. To investigate the diagnostic value of the model SCP, the SCP was validated by applying it to a second, independent, AD and DLB cohort (AD, $n = 34$; DLB, $n = 29$). Mean SCP expressions differed between AD and DLB ($F_{1,64} = 36.2$, $P < 0.001$) with good diagnostic accuracy (receiver operating characteristic (ROC) curve area 0.87, sensitivity 81%, specificity 88%). Forward application of the model SCP to the independent cohort revealed similar differences between groups ($F_{1,61} = 38.4$, $P < 0.001$), also with good diagnostic accuracy (ROC 0.86, sensitivity 80%, specificity 80%). Multivariate analysis of blood flow SPECT data appears to be robust and shows good diagnostic accuracy in two independent cohorts for distinguishing DLB from AD.

*Journal of Cerebral Blood Flow & Metabolism* (2013) **33,** 612–618; doi:10.1038/jcbfm.2013.2; published online 30 January 2013

**Keywords:** Alzheimer's disease; differential diagnosis; dementia with Lewy bodies; perfusion; spatial covariance; SPECT

## INTRODUCTION

Dementia with Lewy bodies (DLB) is the second most common form of neurodegenerative dementia after Alzheimer's disease (AD), with diagnosis based on revised consensus criteria.[1] Histopathologically, DLB is characterized by the presence of cortical and subcortical Lewy bodies while clinically the core diagnostic features of DLB are (1) recurrent visual hallucinations that are typically well-formed and detailed, (2) cognitive fluctuations with variations in attention and alertness, and (3) spontaneous motor features of parkinsonism. The presence of two or three of these core signs is sufficient for a diagnosis of probable DLB.[1] However, distinguishing DLB from AD continues to be difficult because of overlapping clinical and neuropathological features.[2,3] Nevertheless, the accurate identification and differentiation of DLB and AD is particularly important as this affects patient management. Those with DLB exhibit adverse sensitivity to neuroleptics, a positive response to cholinesterase inhibitors especially for noncognitive symptoms[4] and, compared with AD, a different prognosis.[5,6] Methods that can improve the diagnostic accuracy of DLB and AD are therefore of great value. Dopaminergic imaging is one approach that has been widely studied, and yields sensitivity of 75% to 80% and specificity of 90%.[7,8] However, it still has relatively limited availability, requires thyroid blocking, and a 3-hour wait between injection and imaging, and can misdiagnose at least 20% of DLB cases.[7] In addition, it may not suitable for all subjects and other biomarkers of similar or higher diagnostic accuracy is needed.

Studies investigating group differences in regional cerebral blood flow (rCBF) between DLB and AD using single-photon emission computed tomography (SPECT) imaging have broadly reported consistent results. Using region of interest methods, occipital, frontal, and parietal lobe perfusion deficits have been observed in DLB relative to AD, with relative preservation of temporal lobe perfusion.[9–11] Using voxelwise procedures, reduced rCBF in occipital cortex as well as in the precuneus has been shown in DLB compared with AD.[12–14] Results from visual rating are less consistent,[15,16] with some even reporting similar patterns of hypoperfusion between DLB and nonDLB cases.[17] Quantitative uptake measures in specific brain regions have also been used as markers to assess diagnostic performance of perfusion SPECT imaging in distinguishing DLB from AD. Using medial occipital lobe uptake as the classification variable, sensitivity in diagnosing DLB ranged from 75% to 85% while specificity in detecting AD was 78% to 85%.[13,14] Studies that used multiple ROIs in discriminant functions have also been explored, but results have been variable (sensitivity 65% to 90%, specificity 64% to 80%).[9–11]

[1]Institute for Ageing and Health, Newcastle University, Campus for Ageing and Vitality, Newcastle upon Tyne, UK; [2]Regional Medical Physics Department, Royal Victoria Infirmary, Newcastle upon Tyne, UK and [3]Department of Psychiatry, University of Cambridge, Cambridge, UK. Correspondence: Dr SJ Colloby, Institute for Ageing and Health, Newcastle University, Campus for Ageing and Vitality, Newcastle upon Tyne NE4 5PL, UK.
E-mail: sean.colloby@ncl.ac.uk
This work was supported by the Medical Research Council UK (grant number G9817682), and by the National Institute for Health Research (NIHR) Research for Public Benefit, Wellcome Trust (Fellowship funding for J-PT), NIHR Newcastle Biomedical Research Centre in Ageing and Chronic Disease and Biomedical Research Unit in Lewy Body Dementia based at Newcastle upon Tyne Hospitals NHS Foundation Trust and Newcastle University and the NIHR Dementia Biomedical Research Unit at Cambridge University Hospitals NHS Foundation Trust and the University of Cambridge. The views expressed are those of the author(s) and not necessarily those of the NHS, the NIHR or the Department of Health.
Received 6 November 2012; revised 14 December 2012; accepted 3 January 2013; published online 30 January 2013

Therefore, while there is general consensus that group differences in rCBF exist between AD and DLB, the accuracy of single measures and discriminant functions and how these markers can be generalized and applied to independent populations in diagnosing individual subjects with AD and DLB is still unclear.

Quantification methods in evaluating perfusion brain SPECT deficits between AD and DLB have largely adopted a univariate approach that treats each ROI or voxel as an independent measure across brain regions, and ignores the extensive functional and structural connections between them. An alternative method, a multivariate perspective, which determines the spatial covariance of a set of images, overcomes the concept of functional segregation and provides important information regarding the interactions between brain regions. One form of voxel spatial covariance analysis (SCA) is the scaled subprofile model,[18] an extension of principal component analysis (PCA), which generate a series of PCA eigenimages of brain uptake representing significant sources of variance in the data that may also reflect specific disease characteristics. These procedures have previously been applied to positron emission tomography and SPECT images in neurodegenerative disorders such as Parkinson's disease[19–21] and AD.[22–24]

Because of differences between DLB and AD in terms of their clinical and cognitive presentation, and differences in patterns of rCBF based on more traditional methods of analysis, the aim of the present study was to examine $^{99m}$Tc-exametazime SPECT images with a voxel SCA approach, to identify a voxel spatial covariance pattern (SCP) that differentiated DLB from AD. The validity of the derived pattern was then tested by application to an independent AD and DLB cohort. We hypothesized that multivariate methods would lead to greater diagnostic discrimination between groups than previously published univariate methods.

## MATERIALS AND METHODS

### Subjects

The study populations consisted of two distinct DLB and AD cohorts: a model derivation sample (40 AD, 26 DLB) and an independent test or validation group (34 AD, 29 DLB). All subjects were recruited from a community-dwelling population who had been referred to local old age psychiatry, neurology or geriatric medicine services and studies were approved by the local research ethics committee and UK Department of Health's Administration of Radioactive Substances Advisory Committee. All participants and the nearest relative (for patients who lacked capacity) gave informed written consent. All individuals underwent detailed physical, neurologic, and neuropsychiatric examinations, which included history, mental state, and physical examination. Investigations included routine hematology and biochemistry screening, thyroid function tests, syphilis serology, vitamin $B_{12}$ and folate levels, chest X-ray, and head CT scan. Global cognitive function was tested using the mini-mental state examination (MMSE).[25] Parkinsonism was rated using the motor subsection of the Unified Parkinson's Disease Rating Scale (UPDRS III).[26] Diagnosis of patients was undertaken before (and therefore blind to) SPECT imaging using the NINCDS-ADRDA criteria for AD,[27] and for DLB, the original (independent cohort) and revised (derivation cohort) consensus criteria's.[1,28] For the model derivation sample: 40 patients were diagnosed as 'probable' AD and 26 patients as 'probable' DLB. The independent validation group comprised: 4 neuropathologically confirmed, 28 'probable' and 2 'possible' AD; and 7 neuropathologically confirmed, 18 'probable' and 4 'possible' DLB.

### $^{99m}$Tc-Exametazime Single-Photon Emission Computed Tomography Scanning

*Model derivation sample*. Patients were scanned using a double-headed gamma camera (Siemens Symbia S, Erlangen, Germany) fitted with a low-energy high-resolution parallel hole collimator within 30 minutes after a bolus intravenous injection of 500 MBq of $^{99m}$Tc-exametazime (Ceretec, GE Healthcare, Amersham, UK). One hundred and twenty (60 per detector) 25 seconds views over a 360° orbit were acquired on a $128 \times 128$ matrix, pixel and slice thickness 3.9 mm. Imaging time was 25 minutes. Images were reconstructed using filtered backprojection with a Butterworth filter (order 8, cutoff 0.35 cycles/cm). Axial resolution was 12 mm full width at half maximum. Reconstructed images were corrected for gamma ray attenuation using Chang's algorithm (uniform attenuation coefficient, $\mu = 0.14$/cm). Scatter correction was not applied.

*Independent test sample*. Patients were scanned using a triple-headed rotating gamma camera (Picker 3000XP, Picker, North Rhine-Westphalia, Germany) fitted with a high-resolution fan-beam collimator, ~10 minutes after a bolus intravenous injection of 500 MBq of $^{99m}$Tc-exametazime. Three hundred and sixty (120 per detector) 15 second views over $3 \times 360°$ orbit were acquired on a $128 \times 128$ matrix with a pixel and slice thickness of 3.5 mm. Imaging time was 30 minutes. Axial resolution was 12 mm full width at half maximum. Images were reconstructed using filtered backprojection with a Butterworth filter (order 13, cutoff 0.2 cycles/cm). Reconstructed images were corrected for gamma ray attenuation using Chang's algorithm (uniform attenuation coefficient, $\mu = 0.11$/cm). Scatter correction was not applied.

Within 3 months of their $^{99m}$Tc-exametazime scan the majority of patients in the independent test sample (AD, $n = 31$; DLB, $n = 27$) also underwent an $^{123}$I-FP-CIT (DaTSCAN, GE Healthcare) SPECT scan. Acquisition and processing of scans have been previously outlined.[8]

### Spatial Preprocessing

All images from both data sets were spatially normalized using an affine transform (12 parameters) to match a $^{99m}$Tc-exametazime SPECT template in standard MNI (Montreal Neurological Institute; http://www.bic.mni.mcgill.ca/) space using FMRIB's linear image registration tool (http://www.fmrib.ox.ac.uk/fsl/flirt/index.html). Generation of the template image has been previously described.[15] Images were then visually inspected to ensure accuracy of registrations. Next, a 16-mm full width at half maximum 3D Gaussian filter was applied to the registered scans, producing spatially smoothed images. Lastly, scans were intensity scaled to their mean whole-brain uptake defined from an SPECT binary mask image.

### Multivariate Spatial Covariance Analysis

Voxel-based scaled subprofile model/PCA was simultaneously applied to the preprocessed images of the derivation sample (AD, $n = 40$; DLB, $n = 26$) using the generalized covariance analysis software suite (http://www.nitrc.org/projects/gcva_pca/).[29] This captured the major sources of between and within group variation. An SPECT binary mask image defined the brain volume subspace for voxelwise analyses. This generated a series of 66 PCA eigenimages that were organized in a decreasing order of variance for each subsequent eigenimage. Voxels participating in each eigenimage may have either positive or negative weights, where the weights express the strength of interaction between voxels that contribute to the eigenimage. Voxels with positive and negative weighting can be interpreted as exhibiting concomitant increased and decreased blood flow, respectively. Once calculated, eigenimage weights were fixed and equal for all subjects. The degree to which a subject expressed each $\text{eigenimage}_{\{i=1\ldots66\}}$ was by means of a subject scaling factor ($\text{SSF}_{\{i=1\ldots66\}}$), where a higher SSF score represents more concurrent increased flow of voxels with positive weights and more concurrent decreased flow of voxels with negative weights.

To identify an SCP that best-discriminated DLB from AD, each individual's $\text{SSFs}_{\{i=1\ldots66\}}$ were entered into a linear regression model as predictor variables with group membership (DLB versus AD) as the dependent variable. Akaike's information criteria was used to determine how many $\text{eigenimages}_{\{i\}}$ should be included in the regression to achieve optimal bias-variance trade-off.[30] Eigenimages {1, 2, 3, 6, 7, and 11}, which initially captured 44.1% of the total data variance, produced the lowest value of Akaike's information criterion and were selected as predictors for the regression model. The resulting linear combination of these eigenimages generated the model SCP that optimally distinguished DLB from AD, accounting for up to 13.8% of the total data variance. The degree to which each subject expressed the model SCP was represented by the $\text{SSF}_{\{\text{model\_SCP}\}}$, and used as the multivariate imaging marker.

To investigate the diagnostic value of the model SCP in discriminating DLB from AD, the SCP was applied then to the independent AD and DLB test sample (AD, $n = 34$; DLB, $n = 29$). This was performed by operation of forward application, where every voxel in a subject scan is multiplied by the corresponding voxel weight in the SCP and summed over the brain volume subspace defined by the SPECT binary mask image. The resultant number denotes to what extent a subject characterizes the model SCP.

Using this technique, each individual's SSF of the model SCP was computed $SSF_{\{model\_SCP\}}$.

### Univariate Analysis

The spatially preprocessed images of the derivation sample were then investigated on a voxelwise univariate basis using statistical parametric mapping (SPM8; http://www.fil.ion.ucl.ac.uk/spm) and MATLAB 7.9 (Mathworks, Cambridge, UK). Differences in rCBF between DLB and AD were assessed using the general linear model (two-sample *t*-test) in SPM8. The SPECT binary mask image defined the voxels for analysis. Results were corrected for multiple comparisons using the FWE (familywise error) threshold of $P_{FWE} \leqslant 0.05$.

### Statistical Analyses

Data were exported into the Statistical Package for Social Sciences software (SPSS version 19.0, http://www-01.ibm.com/software/analytics/spss/products/statistics/) for further statistical evaluation. Continuous variables were tested for normality of distribution using the Shapiro-Wilk test and visual inspection of variable histograms. Differences in demographic, clinical, and imaging variables were examined where appropriate using parametric (ANOVA) and nonparametric ($\chi^2$, Mann–Whitney U) tests. Diagnostic characteristics of the SCP expressions in distinguishing DLB from AD was determined from receiver operating characteristic (ROC) curve analysis.[31] All statistical tests were reported as significant if $P \leqslant 0.05$.

## RESULTS

### Subject Demographics and Clinical Characteristics

Table 1 shows demographic and clinical characteristics of the derivation and independent populations. Both data sets exhibited similar profiles between AD and DLB, where groups were matched for gender, age, MMSE, and Cambridge Cognitive Examination (CAMCOG). Motor scores (UPDRS III) were, as expected, significantly higher in DLB than in AD.

### Multivariate Spatial Covariance Analysis

The voxel SCP identified with multivariate SCA in distinguishing DLB from AD is presented in Figure 1A. Negative weights (concomitant decreased rCBF) were observed bilaterally in medial temporal, putamen, thalamus, medial orbitofrontal, superior frontal, and pre/post central regions as well as in pons/midbrain and anterior cerebellum. Positive weights (concomitant increased rCBF) were observed bilaterally in caudate, lingual, precuneus, occipital; middle frontal, anterior, and posterior cingulate as well as unilaterally in right superior temporal, right middle temporal, and right posterior cerebellum. The SCP expression scores ($SSF_{\{model\_SCP\}}$), representing the extent to which a subject expresses the topography, were significantly higher in AD than in DLB ($F_{1,64} = 36.2$, $P < 0.001$). Figure 1B shows the distribution of $SSF_{\{model\_SCP\}}$ scores in these groups (mean ± s.d., AD = 3.25 ± 1.92, DLB = 0.22 ± 2.11). The ROC curve analysis was then used to determine the diagnostic value of using $SSF_{\{model\_SCP\}}$ scores in classifying AD and DLB according to clinical diagnosis. Diagnostic characteristics (ROC curve area ± standard error, 'optimal' sensitivity and specificity) was (0.87 ± 0.05, 81%, 88%), indicating 'very good' accuracy.

**Table 1.** Demographic and clinical characteristics of the derivation and independent cohorts

| | *AD* | *DLB* | P *value* |
|---|---|---|---|
| *Derivation* | | | |
| *n* | 40 | 26 | |
| Gender (m:f) | 24:16 | 19:7 | $\chi^2 = 1.2$, $P = 0.3$ |
| Age (years) | 75.7 ± 7.3 | 75.9 ± 5.2 | $F_{1,64} = 0.03$, $P = 0.9$ |
| MMSE ($_{max}$. 30) | 21.0 ± 3.6 | 21.5 ± 4.5 | $F_{1,64} = 0.2$, $P = 0.6$ |
| CAMCOG ($_{max}$. 107) | 71.1 ± 11.3 | 70.6 ± 15.9 | $F_{1,64} = 0.02$, $P = 0.9$ |
| UPDRS III ($_{max}$. 108) | 3.6 ± 3.2 | 25.4 ± 13.0 | $U =$ **992.0,** $P <$ **0.001** |
| *Independent* | | | |
| *n* | 34 | 29 | |
| Gender | 13:21 | 17:12 | $\chi^2 = 2.6$, $P = 0.1$ |
| Age | 78.6 ± 5.6 | 75.7 ± 6.8 | $F_{1,61} = 3.5$, $P = 0.07$ |
| MMSE | 17.5 ± 4.8 | 16.3 ± 5.5 | $F_{1,61} = 0.9$, $P = 0.4$ |
| CAMCOG | 58.5 ± 15.4 | 60.7 ± 14.5 | $F_{1,61} = 0.33$, $P = 0.6$ |
| UPDRS III | 5.7 ± 5.3 | 26.9 ± 15.0 | $U =$ **899.0,** $P <$ **0.001** |

AD, Alzheimer's disease; DLB, dementia with Lewy bodies; MMSE, minimental state examination; CAMCOG, Cambridge Cognitive Examination; UPDRS, Unified Parkinson's Disease Rating Scale. Values expressed as mean ± 1s.d. Bold text denotes significant differences.

### Forward Application to the Independent Alzheimer's Disease Dementia with Lewy Bodies Cohort

When the model SCP was forwardly applied to the independent AD DLB groups, pattern expressions were once again significantly higher in AD than in DLB ($F_{1,61} = 38.4$, $P < 0.001$; mean ± s.d., AD = 4.69 ± 2.80, DLB = 0.13 ± 3.04). The ROC curve analysis

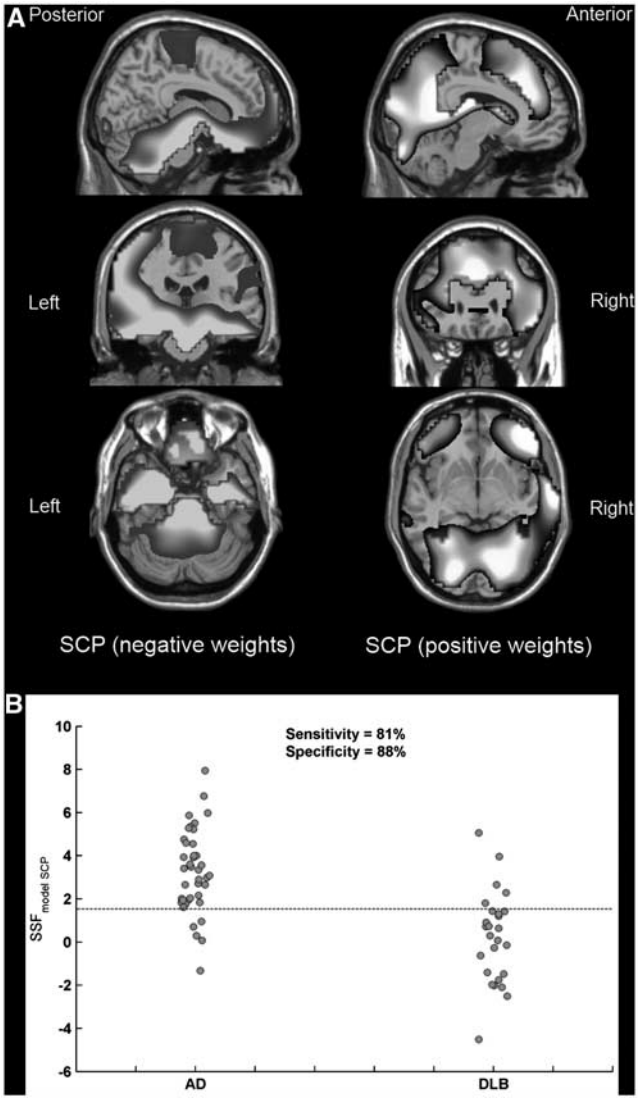


**Figure 1.** Orthogonal views of the spatial covariance pattern (SCP) that differentiates Alzheimer's disease (AD) and dementia with Lewy bodies (DLB) superimposed onto a magnetic resonance imaging (MRI) template (**A**). Distribution of $SSF_{\{model\_SCP\}}$ scores in AD ($n = 40$) and DLB ($n = 26$) (**B**). Reference line denotes the threshold for 'optimum' DLB sensitivity and AD specificity. SSF, subject scaling factor.

revealed 'optimal' diagnostic characteristics of 0.86 ± 0.05, 80%, and 80%, respectively, showing 'very good' accuracy in classifying AD and DLB in line with clinical diagnosis. However, to simulate the realistic context of a clinical application on a subject-by-subject basis, we used the decision threshold that gave the optimal sensitivity and specificity in the derivation sample. Therefore, the 'clinically meaningful' scores were DLB sensitivity 72% and AD specificity 88%. Figure 2 shows the scatter of $SSF_{\{model\_SCP\}}$ scores in the independent sample, while cases above and below the reference line were classified as 'multivariate AD' and 'multivariate DLB', respectively.

### Comparison Between Multivariate Spatial Covariance Analysis and $^{123}$I-FP-CIT Imaging in Diagnosing Alzheimer's Disease and Dementia with Lewy Bodies

For the independent AD DLB cohort, subjects with both $^{99m}$Tc-exametazime and $^{123}$I-FP-CIT SPECT scans (AD, $n = 31$; DLB, $n = 27$) were compared with respect to their diagnostic performance in classifying AD and DLB in line with clinical diagnosis. For $^{123}$I-FP-CIT, a consensus visual rating score was used as the classification variable as previously reported.[8,15] The ROC curve analysis revealed diagnostic characteristics of (0.80 ± 0.06, 72%, 90%) and (0.83 ± 0.06, 81%, 84%) for the multivariate SCA approach and $^{123}$I-FP-CIT visual rating, respectively, indicating similar diagnostic accuracy in this cohort ($\Delta = 0.02 \pm 0.09$, $Z = 0.3$, $P = 0.80$). Table 2 depicts the association between $^{123}$I-FP-CIT imaging and the multivariate SCA measures in classifying AD and DLB using clinical diagnosis as the 'gold' standard. There were five AD and five DLB subjects misdiagnosed using $^{123}$I-FP-CIT imaging; of these, four AD and two DLB were correctly classified by SCA.

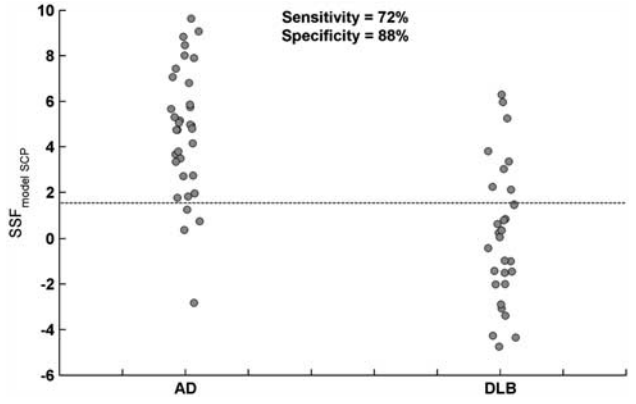


**Figure 2.** Forward application of the model spatial covariance pattern (SCP) to an independent AD DLB cohort. Distribution of $SSF_{\{model\_SCP\}}$ scores in AD ($n = 34$) and DLB ($n = 29$). Reference line denotes the 'clinically meaningful' threshold. Cases above and below the reference line are classified as 'multivariate AD' and 'multivariate DLB', respectively. AD, Alzheimer's disease; DLB, dementia with Lewy bodies; SSF, subject scaling factor.

**Table 2.** The association between FP-CIT SPECT imaging and the multivariate SCA approach in classifying AD and DLB in accordance with clinical diagnosis

| | *AD* (n = *31*) | | *DLB* (n = *27*) | |
|---|---|---|---|---|
| | *FP-CIT positive* | *FP-CIT negative* | *FP-CIT positive* | *FP-CIT negative* |
| Multivariate DLB | 1 | 2 | 17 | 2 |
| Multivariate AD | 4 | 24 | 5 | 3 |

AD, Alzheimer's disease; DLB, dementia with Lewy bodies; MMSE, mini-mental state examination; SCA, spatial covariance analysis; SPECT, single-photon emission computed tomography.

### Correlation of Spatial Covariance Pattern Expression with Demographic and Clinical Variables

For both cohorts, the relationship between SCP expression ($SSF_{\{model\_SCP\}}$) and gender, age, MMSE, CAMCOG, and UPDRS III was investigated separately in AD and DLB. No significant effects were observed between these variables and SCP expression in AD (derivation sample: $r \leqslant 0.1$, $P \geqslant 0.28$; independent sample: $r \leqslant 0.1$, $P \geqslant 0.3$) and DLB ($r \leqslant 0.31$, $P \geqslant 0.06$; $r \leqslant 0.19$, $P \geqslant 0.17$).

### Univariate SPM8 Analyses

Figure 3A illustrates the univariate voxelwise results between AD and DLB using SPM8. A significant reduction in rCBF in AD relative to DLB was observed in the left parahippocampal gyrus (*t*-statistic 5.7, *Z*-score 5.1, cluster-extent$_{\{k\}}$, 194). No significant reductions in rCBF were observed in DLB relative to AD. Mean counts/voxel within the significant cluster were then extracted for all spatially preprocessed images using the SPM toolbox MarsBaR (MARSeille Boîte À Région d'Intérêt).[32] The cluster data were then used as a univariate imaging marker. Figure 3B shows the distribution of mean counts/voxel for the cluster data in the derivation cohort that differed between groups (AD = 45.57 ± 2.34, DLB = 49.08 ± 2.25, $F_{1,64} = 36.4$, $P < 0.001$). Diagnostic characteristics of the imaging marker was (0.86 ± 0.05, 73%, 81%), indicating 'good' diagnostic performance. When applied to the independent sample, significant differences were observed among groups (AD = 43.53 ± 2.81, DLB = 45.83 ± 2.78, $F_{1,61} = 10.6$, $P = 0.002$); however, diagnostic accuracy was lower (0.73 ± 0.06, 31%, 94%). Figure 3C shows the scatter of mean counts/voxel for cluster data applied to the independent sample (reference line denotes the 'clinically meaningful' threshold). Relative to the multivariate approach, significant differences were found between their ROC curve areas ($\Delta = 0.13 \pm 0.06$, $Z = 2.2$, $P = 0.03$), indicating that in this sample, diagnostic accuracy was superior using the multivariate method compared with the univariate approach.

## DISCUSSION

In the present study, a voxel SCP was derived from $^{99m}$Tc-exametazime SPECT scans and was found to significantly differentiate AD from DLB. The pattern (expressed higher in AD than in DLB) comprising a linear combination of six eigenimages that accounted for up to 13.8% of the total data variance, where each eigenimage exhibited brain voxels with high spatial covariance. The voxel SCP showed concomitant decreased rCBF in medial temporal, subcortical, medial orbitofrontal, superior frontal, post central, pons, midbrain, and anterior cerebellum. It also revealed concomitant increased rCBF in occipital, precuneus, middle frontal, cingulate, superior and middle temporal and posterior cerebellum. The SCP broadly characterizes concurrent hypoperfusion of the medial temporal lobes with relative preservation of posterior structures including occipital and precuneus in AD relative to DLB. Expressions of SCP were then used as a classification variable in diagnosing AD and DLB according to clinical diagnosis, where results revealed very good diagnostic performance (DLB sensitivity 81%, AD specificity 88%). Validity of the model SCP was investigated by forward application of the derived pattern to an independent AD DLB cohort, where the pattern expression was also found to be significantly different between AD and DLB (AD > DLB). Diagnostic performance of the model SCP on the test cohort showed a consistent level of discrimination between DLB and AD (clinically meaningful values:

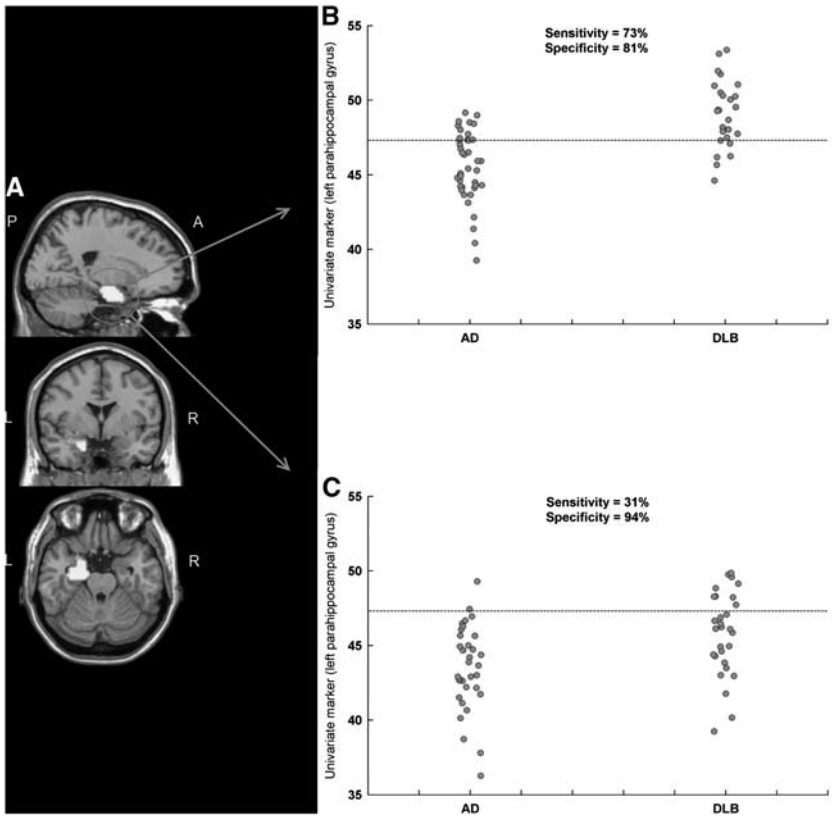


**Figure 3.** Univariate SPM8 results ($P_{FWE} \leqslant 0.05$) superimposed on a magnetic resonance imaging (MRI) template (**A**). The significant region of interest (ROI) cluster was chosen as a univariate marker and applied to the model derivation (**B**) and independent test (**C**) AD DLB cohorts. Reference lines denote the 'clinically meaningful' threshold. AD, Alzheimer's disease; DLB, dementia with Lewy bodies; FWE, familywise error.

DLB sensitivity 72%, AD specificity 88%). The relationship between SCP expression and gender, age, MMSE, CAMCOG, and UPDRS III did not reveal any significant correlations in AD or DLB for either cohort. This suggests either that cognitive measures may have lacked sensitivity or that the SCP may not reflect dementia or motor severity. Univariate analysis of the derivation cohort showed a significant perfusion deficit in the left parahippocampal gyrus in AD relative to DLB which in turn was used as a univariate imaging marker. Diagnostic characteristics on the derivation sample were as expected 'good'; however, when applied to the independent sample, diagnostic performance was much less accurate, especially in DLB. The findings suggest that in these cohorts, the multivariate method was superior to the univariate approach in classifying AD and DLB. Others have also revealed the superior diagnostic utility of the multivariate SCA approach over univariate procedures in diagnosing AD from healthy individuals using $^{18}$F-fluorodeoxyglucose positron emission tomography imaging.[22]

The diagnostic role of perfusion brain SPECT in differentiating DLB from AD has been investigated with occipital rCBF uptake chosen as the classification variable. The studies showed a variable DLB sensitivity and AD specificity of 65% to 85% and 71% to 87%, respectively.[10,11,13,14,33] Studies using $^{18}$F-fluorodeoxyglucose positron emission tomography have largely shown greater diagnostic accuracy than perfusion SPECT in distinguishing DLB from AD.[34,35] The DLB sensitivity and AD specificity are quoted as ranging from 86% to 92% and from 80% to 92%, respectively, although such results should be viewed with caution because of the relatively small samples studied and indeed larger more recent AD DLB positron emission tomography study was found to be less accurate (sensitivity 64%, specificity 65%).[36] $^{123}$I-MIBG, a myocardial scintigraphic SPECT tracer that detects early disturbances of the sympathetic nervous system, has shown excellent diagnostic performance in DLB in selected samples. Hanyu *et al*[33] revealed high diagnostic accuracy in DLB and AD (sensitivity 100%, specificity 92%), while a recent meta analysis showed a pooled DLB sensitivity of 98% and nonDLB specificity of 94%,[37] although these authors indicated that while showing promise, further research with $^{123}$I-MIBG in multicenter cohorts with neuropathological confirmation is required to confirm the high diagnostic accuracy of MIBG scintigraphy in DLB.

Dopaminergic $^{123}$I-FP-CIT SPECT is, perhaps, the most established diagnostic tool in the differential diagnosis of DLB and AD. A study of autopsy confirmed cases reported DLB sensitivity 88% and nonDLB specificity 100%.[38] For antemortem cases, DLB sensitivity of 78% and AD specificity of 88% were observed,[8] while a mean DLB sensitivity of 78% and mean nonDLB specificity of 90% were concluded from a multicenter study.[7] Interestingly, a similar degree of diagnostic accuracy was found in the present study between the multivariate approach of blood flow data and $^{123}$I-FP-CIT visual rating in a sample that included most of the independent AD and DLB cohort. While FP-CIT remains the best-validated imaging biomarker for DLB to date, and so the 'gold standard', the multivariate approach clearly shows great promise and, if replicated by others, may prove a useful alternative to FP-CIT imaging if such imaging is not available. Interestingly, in the independent cohort where both FP-CIT and perfusion SPECT data were available (31 AD and 27 DLB), a subject with two positive test results (multivariate DLB, positive FP-CIT) was 19.5 times ($P < 0.001$) more likely to be DLB than AD. Similarly, a subject with two negative test results (multivariate AD, negative FP-CIT) was 7.0 times ($P < 0.001$) more likely to be AD than DLB. Therefore, there may also be some utility in having both diagnostic tests that would perhaps increase diagnostic

confidence in DLB, although clearly a larger independent prospective cohort study using both of these diagnostic tests would be required to confirm this.

Advantages of the present study include: relatively large DLB populations in the derivation and independent cohorts, validation of the SCP approach on an independent data set, and the availability of FP-CIT imaging in this cohort. Potential weaknesses were the low numbers of autopsy confirmed diagnoses and therefore the reliance on clinical diagnosis as the 'gold standard'. The SCP model was derived from unbalanced AD ($n = 40$) and DLB ($n = 26$) samples, which may to some extent have biased the model toward AD; therefore unsurprisingly, the clinically relevant AD specificity in the independent cohort remained consistent while DLB sensitivity was slightly reduced. A model generated from balanced samples could 'optimize' case detection in that cohort. There were also a number of clinically diagnosed 'possible' AD and DLB cases in the independent sample (two AD and four DLB). However, all but one of these 'possible' cases lay within one standard deviation of their respective group averages and thus we expect that inclusion of such cases would not have significantly altered the conclusions drawn from results of the independent data set. We previously reported the diagnostic utility of covariance $^{99m}$Tc-exametazime SPECT in AD and DLB using an ROI approach that included, in part, the independent cohort of the current study.[39] However for the present study, the addition of a new AD DLB cohort and use of voxel-based procedures are in our view, a major step forward in terms of diagnostic performance and visualizing spatial covariance in AD and DLB compared with our earlier work. Future studies containing pooled autopsy confirmed DLB and AD cases from multicenter sites to generate a comprehensive database, could identify an SCP that distinguishes DLB from AD with high confidence. Disease-specific data sets could also be generated to identify other groups including healthy individuals, vascular, or frontotemporal dementia. Additional clinical/cognitive information along with imaging data producing combination markers may also optimize differential diagnosis.

To our knowledge, this is the first study to investigate the diagnostic utility of voxel multivariate analysis of $^{99m}$Tc-exametazime SPECT imaging data in DLB and AD. The technique appears to be more robust and sensitive than univariate analysis and performed well when validated in an independent patient cohort. This approach shows potential and may offer comparable sensitivity to dopaminergic SPECT for the diagnosis of DLB. While dopaminergic imaging remains the imaging biomarker of choice for DLB, if only perfusion SPECT imaging is available, the present method may offer extra information that could improve case detection in AD and DLB. Models derived from autopsy confirmed individuals and tested in much larger cohorts are required to assess the clinical benefit of this procedure.

## DISCLOSURE/CONFLICT OF INTEREST

The authors declare no conflict of interest.

## ACKNOWLEDGEMENTS

The authors thank staff at the Regional Medical Physics Department, Nuclear Medicine Sections, at Newcastle General Hospital and Royal Victoria Infirmary as well as all members of the clinical research teams who helped with patient recruitment. All authors have seen and agree with the contents of the manuscript and guarantee the accuracy of the references.

## REFERENCES

1 McKeith IG, Dickson DW, Lowe J, Emre M, O'Brien JT, Feldman H *et al.* Diagnosis and management of dementia with Lewy bodies: third report of the DLB Consortium. *Neurology* 2005; **65**: 1863–1872.
2 Galasko D. Lewy bodies and dementia. *Curr Neurol Neurosci Rep* 2001; **1**: 435–441.
3 McKeith IG, Fairbairn AF, Perry RH, Thompson P. The clinical diagnosis and misdiagnosis of senile dementia of Lewy body type (SDLT). *Br J Psychiatry* 1994; **165**: 324–332.
4 Aarsland D, Mosimann UP, McKeith IG. Role of cholinesterase inhibitors in Parkinson's disease and dementia with Lewy bodies. *J Geriatr Psychiatry Neurol* 2004; **17**: 164–171.
5 Aarsland D, Perry R, Larsen JP, McKeith IG, O'Brien JT, Perry EK *et al.* Neuroleptic sensitivity in Parkinson's disease and parkinsonian dementias. *J Clin Psychiatry* 2005; **66**: 633–637.
6 McKeith I, Fairbairn A, Perry R, Thompson P, Perry E. Neuroleptic sensitivity in patients with senile dementia of Lewy body type. *BMJ* 1992; **305**: 673–678.
7 McKeith I, O'Brien J, Walker Z, Tatsch K, Booij J, Darcourt J *et al.* Sensitivity and specificity of dopamine transporter imaging with 123I-FP-CIT SPECT in dementia with Lewy bodies: a phase III, multicentre study. *Lancet Neurol* 2007; **6**: 305–313.
8 O'Brien JT, Colloby SJ, Fenwick J, Williams ED, Firbank M, Burn D *et al.* Dopamine transporter loss visualized with FP-CIT SPECT in the differential diagnosis of dementia with lewy bodies. *Arch Neurol* 2004; **61**: 919–925.
9 Defebvre LJ, Leduc V, Duhamel A, Lecouffe P, Pasquier F, Lamy-Lhullier C *et al.* Technetium HMPAO SPECT study in dementia with Lewy bodies, Alzheimer's disease and idiopathic Parkinson's disease. *J Nucl Med* 1999; **40**: 956–962.
10 Lobotesis K, Fenwick JD, Phipps A, Ryman A, Swann A, Ballard C *et al.* Occipital hypoperfusion on SPECT in dementia with Lewy bodies but not AD. *Neurology* 2001; **56**: 643–649.
11 Pasquier J, Michel BF, Brenot-Rossi I, Hassan-Sebbag N, Sauvan R, Gastaut JL. Value of (99m)Tc-ECD SPET for the diagnosis of dementia with Lewy bodies. *Eur J Nucl Med Mol Imaging* 2002; **29**: 1342–1348.
12 Colloby SJ, Fenwick JD, Williams ED, Paling SM, Lobotesis K, Ballard C *et al.* A comparison of (99 m)Tc-HMPAO SPET changes in dementia with Lewy bodies and Alzheimer's disease using statistical parametric mapping. *Eur J Nucl Med Mol Imaging* 2002; **29**: 615–622.
13 Hanyu H, Shimizu S, Hirao K, Kanetaka H, Sakurai H, Iwamoto T *et al.* Differentiation of dementia with Lewy bodies from Alzheimer's disease using Mini-Mental State Examination and brain perfusion SPECT. *J Neurol Sci* 2006; **250**: 97–102.
14 Shimizu S, Hanyu H, Kanetaka H, Iwamoto T, Koizumi K, Abe K. Differentiation of dementia with Lewy bodies from Alzheimer's disease using brain SPECT. *Dement Geriatr Cogn Disord* 2005; **20**: 25–30.
15 Colloby SJ, Firbank MJ, Pakrasi S, Lloyd JJ, Driver I, McKeith IG *et al.* A comparison of $^{99m}$Tc-exametazime and 123I-FP-CIT SPECT imaging in the differential diagnosis of Alzheimer's disease and dementia with Lewy bodies. *Int Psychogeriatr* 2008 1–17.
16 Donnemiller E, Heilmann J, Wenning GK, Berger W, Decristoforo C, Moncayo R *et al.* Brain perfusion scintigraphy with 99mTc-HMPAO or $^{99m}$Tc-ECD and $^{123}$I-beta-CIT single-photon emission tomography in dementia of the Alzheimer-type and diffuse Lewy body disease. *Eur J Nucl Med Mol Imaging* 1997; **24**: 320–325.
17 Kemp PM, Hoffmann SA, Tossici-Bolt L, Fleming JS, Holmes C. Limitations of the HMPAO SPECT appearances of occipital lobe perfusion in the differential diagnosis of dementia with Lewy bodies. *Nucl Med Commun* 2007; **28**: 451–456.
18 Alexander GE, Moeller JR. Application of the scaled subprofile model to functional imaging in neuropsychiatric disorders: a principal component approach to modeling brain function in disease. *Hum Brain Mapp* 1994; **2**: 79–94.
19 Asanuma K, Tang C, Ma Y, Dhawan V, Mattis P, Edwards C *et al.* Network modulation in the treatment of Parkinson's disease. *Brain* 2006; **129**: 2667–2678.
20 Eckert T, Van Laere K, Tang C, Lewis DE, Edwards C, Santens P *et al.* Quantification of Parkinson's disease-related network expression with ECD SPECT. *Eur J Nucl Med Mol Imaging* 2007; **34**: 496–501.
21 Moeller JR, Nakamura T, Mentis MJ, Dhawan V, Spetsieres P, Antonini A *et al.* Reproducibility of regional metabolic covariance patterns: comparison of four populations. *J Nucl Med* 1999; **40**: 1264–1269.
22 Habeck C, Foster NL, Perneczky R, Kurz A, Alexopoulos P, Koeppe RA *et al.* Multivariate and univariate neuroimaging biomarkers of Alzheimer's disease. *Neuroimage* 2008; **40**: 1503–1515.
23 Johnson KA, Jones K, Holman BL, Becker JA, Spiers PA, Satlin A *et al.* Preclinical prediction of Alzheimer's disease using SPECT. *Neurology* 1998; **50**: 1563–1571.
24 Scarmeas N, Habeck CG, Zarahn E, Anderson KE, Park A, Hilton J *et al.* Covariance PET patterns in early Alzheimer's disease and subjects with cognitive impairment but no dementia: utility in group discrimination and correlations with functional performance. *Neuroimage* 2004; **23**: 35–45.
25 Folstein MF, Folstein SE, McHugh PR. 'Mini-mental state'. A practical method for grading the cognitive state of patients for the clinician. *J Psychiatr Res* 1975; **12**: 189–198.
26 Fahn S, Elton RL, Marsden CD, Goldstein M. Unified Parkinson's disease rating scale. *Recent Developments in Parkinson's Disease*. Macmillan Healthcare: Florham Park, NJ, 1987, Vol II: 153–163.

27 McKhann G, Drachman D, Folstein M, Katzman R, Price D, Stadlan EM. Clinical diagnosis of Alzheimer's disease: report of the NINCDS-ADRDA Work Group under the auspices of Department of Health and Human Services Task Force on Alzheimer's Disease. *Neurology* 1984; **34**: 939–944.
28 McKeith IG, Galasko D, Kosaka K, Perry EK, Dickson DW, Hansen LA *et al.* Consensus guidelines for the clinical and pathologic diagnosis of dementia with Lewy bodies (DLB): report of the consortium on DLB international workshop. *Neurology* 1996; **47**: 1113–1124.
29 Habeck C, Krakauer JW, Ghez C, Sackeim HA, Eidelberg D, Stern Y *et al.* A new approach to spatial covariance modeling of functional brain imaging data: ordinal trend analysis. *Neural Comput* 2005; **17**: 1602–1645.
30 Burnham KP, Anderson DR. *Model Selection and Multimodel Inference*. Springer Verlag: New York, 2002.
31 Zweig MH, Campbell G. Receiver operating characteristic (roc) plots - a fundamental evaluation tool in clinical medicine. *Clinl Chem* 1993; **39**: 1589–1589.
32 Brett M, Anton J-L, Valabregue R, Poline JB. Region of interest analysis using an SPM toolbox [CD-Rom]. *Neuroimage* 2002; **6**.
33 Hanyu H, Shimizu S, Hirao K, Kanetaka H, Iwamoto T, Chikamori T *et al.* Comparative value of brain perfusion SPECT and [(123)I]MIBG myocardial scintigraphy in distinguishing between dementia with Lewy bodies and Alzheimer's disease. *Eur J Nucl Med Mol Imaging* 2006; **33**: 248–253.
34 Ishii K, Imamura T, Sasaki M, Yamaji S, Sakamoto S, Kitagaki H *et al.* Regional cerebral glucose metabolism in dementia with Lewy bodies and Alzheimer's disease. *Neurology* 1998; **51**: 125–130.
35 Minoshima S, Foster NL, Sima AAF, Frey KA, Albin RL, Kuhl DE. Alzheimer's disease versus dementia with Lewy bodies: cerebral metabolic distinction with autopsy confirmation. *Ann Neurol* 2001; **50**: 358–365.
36 Gilman S, Koeppe RA, Little R, An H, Junck L, Giordani B *et al.* Differentiation of Alzheimer's disease from dementia with Lewy bodies utilizing positron emission tomography with $^{[18F]}$fluorodeoxyglucose and neuropsychological testing. *Exp Neurol* 2005; **191**(Suppl 1): S95–S103.
37 Treglia G, Cason E. Diagnostic performance of myocardial innervation imaging using MIBG scintigraphy in differential diagnosis between dementia with lewy bodies and other dementias: a systematic review and a meta-analysis. *J Neuroimaging* 2012; **22**: 111–117.
38 Walker Z, Jaros E, Walker RW, Lee L, Costa DC, Livingston G *et al.* Dementia with Lewy bodies: a comparison of clinical diagnosis, FP-CIT single photon emission computed tomography imaging and autopsy. *J Neurol Neurosurg Psychiatry* 2007; **78**: 1176–1181.
39 Colloby SJ, Taylor JP, Firbank MJ, McKeith IG, Williams ED, O'Brien JT. Covariance 99mTc-exametazime SPECT patterns in Alzheimer's disease and dementia with Lewy bodies: utility in differential diagnosis. *J Geriatr Psychiatry Neurol* 2010; **23**: 54–62.